Entropic exponents of grafted lattice stars

E. J. Janse van Rensburg *

Department of Mathematics and Statistics, York University, Toronto, Ontario M3J 1P3, Canada

(Received 19 July 2022; accepted 20 October 2022; published 14 November 2022)

The surface entropic exponents of half-space lattice stars grafted at their central nodes in a hard wall are estimated numerically using the PERM algorithm. In the square half-lattice the exact values of the exponents are verified, including Barber's scaling relation and a generalization for 2-stars with one and two surface loops respectively. This is the relation $\gamma_{211} = 2\,\gamma_{21} - \gamma_{20}$, where γ_{21} and γ_{211} are the surface entropic exponents of a grafted 2-star with one and two surface loops, respectively, and γ_{20} is the surface entropic exponent with no surface loops. This relation is also tested in the cubic half-lattice where surface entropic exponents are estimated up to 5-stars, including many with one or more surface loops. Barber's scaling relation and the relation $\gamma_{3111} = \gamma_{30} - 3\,\gamma_{31} + 3\,\gamma_{311}$ are also tested, where the exponents $\{\gamma_{31}, \gamma_{311}, \gamma_{3111}\}$ are of grafted 3-stars with one, two, or three surface loops, respectively, and γ_{30} is the surface exponent of grafted 3-stars.

DOI: 10.1103/PhysRevE.106.054132

I. INTRODUCTION

The *connectivity* of a polymer network can be represented as an abstract graph $\mathcal{G}$ of nodes and bonds, where the nodes are branching points in the network, and the bonds represent linear polymers joining the nodes into the network. If the network is embedded in a lattice, then it is a model of the connectivity and the topology of a polymer network in the plane or in a thin layer (if the lattice is two dimensional), or in a good solvent (if the lattice is three dimensional).

If a network with connectivity $\mathcal{G}$ is embedded in the (hyper)-cubic lattice $\mathbb{Z}^d$, then the nodes are located on vertices in the lattice, and the bonds are mutual- and self-avoiding walks joining the nodes. These self-avoiding walks are the *branches* of the network. If $\mathcal{G}$ is a star graph, then the branches are called *arms*. The embedding is *uniform* or *monodispersed* if all the branches are walks of the same length.

The lattice embedding is a model that quantifies the entropy of the corresponding polymer network. If $c_n(\mathcal{G})$ is the number of distinct embeddings of the network, counted up to translation (or by fixing a node at the origin), then the usual scaling assumption is

$$c_n(\mathcal{G}) \sim C\, n^{\gamma(\mathcal{G})-1} \mu_d^n, \tag{1}$$

where $\gamma(\mathcal{G})$ is the *entropic exponent* of the network, C is a constant *amplitude*, and μ_d is the *self-avoiding walk growth constant* [1,2] (see Refs. [3,4], and for lattice stars Ref. [5]). The best estimates of the growth constants in the square and cubic lattices are obtained from simulations of the self-avoiding walk, and are [6–8]

$$\mu_2 = \begin{cases} 2.63815853035(2), & [6] \\ 2.63815853032790(3), & [7] \end{cases} \tag{2}$$

$$\mu_3 = 4.684039931(27). \ [8] \tag{3}$$

Uniform lattice star polymers form a particular class of lattice networks that have received significant attention in the literature, at least since the 1980s [3–5,9–12]. If $s_n^{(f)}$ is the number of uniform lattice stars in $\mathbb{Z}^d$ with f arms (these are *f-stars*) with a central node at the origin, then by Eq. (1),

$$s_n^{(f)} \sim C_f\, n^{\gamma_f - 1}\, \mu_d^n, \tag{4}$$

where γ_f is the f-star entropic exponent and C_f is a constant amplitude depending on f and d. High quality numerical results and estimates of the entropic exponents of star polymers were made in references [13–18].

Lattice networks of connectivity $\mathcal{G}$ grafted to a wall have scaling similar to Eq. (1). In the hypercubic half-lattice $\mathbb{Z}_+^d = \{(x_1, x_2, \ldots, x_d) \in \mathbb{Z}^d \mid \text{such that } x_d \geqslant 0\}$ a chosen node of a network is grafted at the origin. Nodes of the network located in the boundary (or hard wall) $\partial\mathbb{Z}_+^d$ of the half-lattice are *surface nodes*. Depending on the connectivity $\mathcal{G}$ such networks may have *loops* (circuits which are lattice polygons) as well as *surface loops* (self-avoiding walks with both endpoints in hard wall $\partial\mathbb{Z}_+^d$ of the half-lattice). For example, in Fig. 1 we show a schematic of a lattice network in $\mathbb{Z}_+^2$ with connectivity to a lattice 3-star without (left) and with (right) a surface loop.

A. Vertex exponents, and entropic exponents

The entropic exponents of networks of connectivity $\mathcal{G}$, in the full lattice, or in the half-lattice, can be expressed in terms of *vertex exponents* σ_f and *surface vertex exponents* σ'_g by [19,20]

$$\gamma_{\mathcal{G}} = 1 + \sum_f m_f \sigma_f + \sum_g m_g \sigma'_g - c(\mathcal{G})\, d\nu - \ell(\mathcal{G})\, \nu, \tag{5}$$

where ν is the metric exponent of the self-avoiding walk ($\nu = 3/4$ in two dimensions [21], and $\nu = 0.58759700(40)$ in three dimensions [22]). The coefficient m_g is the number of surface nodes of degree g in $\partial\mathbb{Z}_+^d$, m_f is the number of nodes of degree f in the bulk lattice, $c(\mathcal{G})$ is the number of

*rensburg@yorku.ca

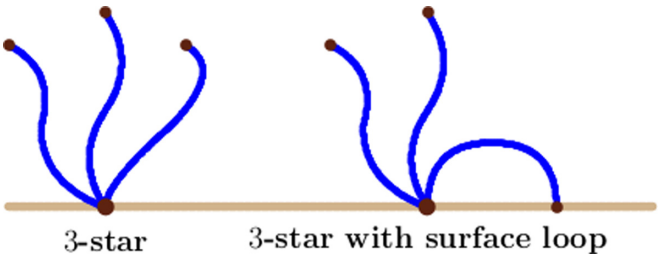

FIG. 1. Schematic of 3-stars in a half-lattice. The central node of the star is attached at the origin in the hard wall (the boundary of the half-lattice). On the right the star has one arm forming a surface loop. The star on the left has no loops or surface loops.

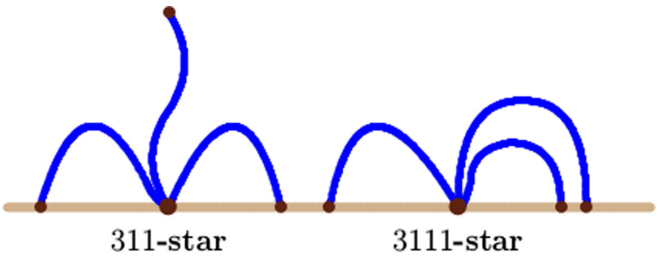

FIG. 2. Schematic illustrations of 311-stars (left) and 3111-stars (right) in a half-lattice. In the half-square lattice, the one arm of the 311-star is "screened" from the hard wall by the other two arms with endpoints in the hard wall. In the case of 3111-stars, all three arms have endpoints in the hard wall, and the only way to accommodate this is by having one arm located inside the surface loop created by the hard wall and an arm. This makes simulations of 3111-stars in the square half-lattice very challenging. In our PERM simulations we rarely observed these states in the 10^9 iterations done.

independent circuits in the network, and $\ell(\mathcal{G})$ is the number of independent surface loops. Testing of Eq. (5) is limited to self-avoiding walks in a half-lattice [23], and for branched networks, to star polymers in bulk [16–18] and a few cases of branched acyclic networks in bulk [17,18].

Exact values of the vertex exponents in two dimensions were calculated using conformal invariance techniques [19,20,24]. These are

$$\sigma_f = \tfrac{1}{64}\,(2-f)\,(9f+2), \quad \text{and} \quad \sigma'_f = \tfrac{1}{32}\,f\,(2-9f). \tag{6}$$

Using these expressions, the exact values of $\gamma_{\mathcal{G}}$ are known in the square lattice. For example, putting $f = 0$ and using Eq. (5) gives the exact value of the entropic exponent of the self-avoiding walk $\gamma = 1 + 2\sigma_1 = 43/32$ [21].

In three dimensions there are ϵ-expansion estimates [25] for the vertex exponents. To first order in ϵ [19],

$$\sigma_f = \tfrac{\epsilon}{16}\,f\,(2-f) + O(\epsilon^2); \tag{7}$$

$$\sigma'_f = -\tfrac{1}{2}\,f + \tfrac{\epsilon}{16}\,f\,(2-f) + O(\epsilon^2). \tag{8}$$

These approximations deteriorate quickly with increasing degrees of the nodes (see for example [18]), but can be used with Eq. (5) to approximate the entropic exponents $\gamma_{\mathcal{G}}$ in three dimensions. In the case of the self-avoiding walk, the first order ϵ-expansion estimate $\gamma = 1+2\sigma_1 \approx 1.125$ compares relatively well with the best numerical estimates $\gamma = 1.15698(34)$ [26] and $\gamma = 1.15695300(95)$ [27]. See Refs. [19,20,28] for $O(\epsilon^2)$, and [29] for $O(\epsilon^4)$, expansions for σ_f.

In this paper the focus is on a lattice star in the half-lattice with its central node at the origin, such as schematically illustrated in Fig. 1. We first introduce notation to distinguish the connectivities of f-stars in the half-lattice $\mathbb{Z}^d_+$ efficiently.

Let $f1^g \equiv f\overbrace{11\ldots1}^{g}$ denote lattice stars in the half-lattice $\mathbb{Z}^d_+$ with a central node of degree f located at the origin in the boundary $\partial\mathbb{Z}^d_+$ (*the hard wall*), and with $g \leqslant f$ arms having their endpoints in the hard wall (and so forming g *surface loops*). For example, in Fig. 1, the cases $31^0 \equiv 30$ (left) and $31^1 \equiv 31$ (right) are shown. Similarly, $31^2 \equiv 311$ denotes 3-stars with a central node at the origin and with two arms having their endpoints in the hard wall (and so forming two surface loops), and $31^3 \equiv 3111$ denotes 3-stars with three surface loops (see Fig. 2).

The entropic exponents of half-lattice stars with connectivity $f1^g$ is denoted by γ_{f1^g}. For example, γ_{311} is the entropic exponent of 3-stars with two arms forming surface loops, and for the cases in Fig. 1, we have γ_{30} (left) and γ_{31} (right). In terms of Eq. (5), the entropic exponent of f-stars with g surface loops in the half-lattice is given by

$$\gamma_{f1^g} = \gamma_{f\underbrace{11\ldots1}_{g}} = 1 + \sigma'_f + (f-g)\,\sigma_1 + g\,\sigma'_1 - g\,\nu. \tag{9}$$

The vertex exponents are given in Eq. (6) in two dimensions, and are approximated in the ϵexpansion in Eqs. (7) and (8) in three dimensions.

In the case of a self-avoiding walk $\gamma = 1+2\sigma_1$, and for a walk from the origin in $\mathbb{Z}^d_+$, $\gamma_1 = 1+\sigma'_1+\sigma_1$ (since $f = 1$ and $g = 0$). If both endpoints are in $\partial\mathbb{Z}^d_+$, then $f = g = 1$ and thus $\gamma_{11} = 1+2\sigma'_1 - \nu$. Eliminating σ_1 and σ'_1 gives Barber's scaling relation [30,31]

$$2\,\gamma_1 - \gamma_{11} = \gamma + \nu. \tag{10}$$

In $d = 2$ the sum of the exact values $\gamma = 43/32$, $\nu = 3/4$ [21] on the right hand side equals the sum of the exact values $\gamma_1 = 61/64$ [32] and $\gamma_{11} = -3/16$ [24] on the left hand side. Numerical results are in agreement with these results, namely $\gamma_1 = 0.945(5)$ and $\gamma_{11} = -0.19(3)$ [31], and $\gamma_1 = 0.9551(3)$ [33]. This shows that $2\,\gamma_1 - \gamma_{11} = 2.08(4)$ while the exact value is $\gamma+\nu = 67/32 = 2.09375\ldots$.

In three dimensions, early estimates $\gamma_1 = 0.687(5)$ and $\gamma_{11} = -0.38(2)$ [34,35], and $\gamma_1 = 0.697(2)$ and $\gamma_{11} = -0.383(5)$ [36], gave way to the more accurate results $\gamma_1 = 0.6786(12)$ and $\gamma_{11} = -0.390(2)$ in Ref. [23]. The best available estimates can be found in Ref. [37] where γ_1 is estimated, and γ_{11} is estimated from the bridge entropic exponent γ_b using the relation $\gamma_b = \gamma_{11} + \nu$ [12]. These are $\gamma_1 = 0.677667(17)$ and $\gamma_{11} = -0.389245(28)$. These values give $2\gamma_1-\gamma_{11} = 1.744579(62)$ and using the best estimates $\gamma = 1.15695300(95)$ [27] and $\nu = 0.58759700(40)$ [22,38], $\gamma+\nu = 1.7445500(14)$. This confirms the Barber scaling relation to very high accuracy. The mean field values of these exponents are $\gamma = 1$, $\nu = 1/2$, $\gamma_1 = 1/2$, and $\gamma_{11} = -1/2$ [39,40].

TABLE I. PERM simulations of f-stars.

Dimension	f	Length	Threads	Iter/Thread	Iterations
$d=2$	1	10000	4	2.5×10^8	10^9
	2	16000	4	2.5×10^8	10^9
	3	15900	4	2.5×10^8	10^9
$d=3$	1	10000	4	2.5×10^8	10^9
	1[a]	10000	8	1.25×10^8	10^9
	2	10000	4	2.5×10^8	10^9
	3	9900	6	1.666×10^8	10^9
	4	10000	4	2.5×10^8	10^9
	5	12500	4	2.5×10^8	10^9

[a]Panneton generator [46].

More generally, one may notice that when $f \geqslant 2$, then the vertex exponents in Eq. (9) can be eliminated by using an alternating sum and binomial coefficients so that

$$\sum_{g=0}^{f}(-1)^g\binom{f}{g}\gamma_{f1^g}=0. \tag{11}$$

This shows, for example, that $\gamma_{20}-2\gamma_{21}+\gamma_{211}=0$ and $\gamma_{30}-3\gamma_{31}+3\gamma_{311}-\gamma_{3111}=0$. The identity

$$\gamma_{20}=\gamma-1 \tag{12}$$

was noted in Ref. [19], and from it and Eq. (11) with $f=2$ it follows that

$$2\gamma_{21}-\gamma_{211}=\gamma-1. \tag{13}$$

This is a generalization of Barber's scaling relation [Eq. (10)]. Noting that $\gamma-1=2\sigma_1$, $\gamma_1-1=\sigma_1+\sigma_1'$, and $\gamma_{20}=\gamma-1=1+\sigma_2'+2\sigma_1$ (see also Ref. [20]) allows one to solve for $\{\sigma_1,\sigma_1',\sigma_2'\}$ from the best numerical estimates in Refs. [12,27] to obtain very accurate estimates for grafted 2-star exponents:

$$\begin{aligned}\gamma_{20}&=0.15695300(95),\\ \gamma_{21}&=-0.909930(17),\\ \gamma_{211}&=-1.976813(33).\end{aligned} \tag{14}$$

These estimates are consistent with Eq. (11).

II. NUMERICAL RESULTS

The numerical approaches developed in Ref. [23] based on the PERM algorithm [16–18,41,42], and in particular the flat histogram [43] and the parallel implementations [44] of PERM, can be used to estimate lattice star entropic exponents in $\mathbb{Z}^d$ (and in $\mathbb{Z}_+^d$) efficiently (see Ref. [23] for half-space self-avoiding walk sampling using PERM). In this paper similar approaches are used, except that in addition to self-avoiding walks grafted at one endpoint in $\partial\mathbb{Z}_+^d$, f-stars are sampled with their central nodes at the origin in $\mathbb{Z}_+^d$. The details of our simulations are shown in Table I. An iteration is a started PERM sequence (which may be pruned and enriched by the algorithm). In these simulations, the Mersenne Twister random number generator [45] was used, except in one case as noted in Table I where the Panneton generator in reference [46] was used instead. In each simulation, the data were sieved by collecting data on stars separately by number of surface loops. Thus, the algorithm produced data on $s_n^{(f)}(g)$, the number of stars with a central node of degree f at the origin in the half-lattice $\mathbb{Z}_+^d$, and with g arms forming surface loops. The scaling of $s_n^{(f)}(g)$ is

$$s_n^{(f)}(g)\sim n^{\gamma_{f1^g}-1}\,\mu_d^n\,(1+B/n+C/n^{\Delta}+\cdots), \tag{15}$$

where Δ is the (first) self-avoiding walk confluent correction exponent which has value $\Delta=3/2$ if $d=2$ [21,47,48] and $\Delta=0.528(8)$ if $d=3$ [22]. Dividing by $\mu_d^n n^{\gamma_{f1^g}-1}$ and taking logarithms give

$$\log\left(\frac{s_n^{(f)}(g)}{\mu_d^n\,n^{\gamma_{f1^g}-1}}\right)=\begin{cases}A+B/n+\cdots, & \text{if } d=2;\\ A+B/n^{\Delta}+\cdots, & \text{if } d=3,\end{cases} \tag{16}$$

where the logarithms on the right hand side were expanded assuming n is large. The best value of γ_{f1^g} and a confidence interval on it can be determined by plotting the left hand side against $1/n$ if $d=2$, and against $1/n^{\Delta}$ if $d=3$. This approach was developed in Ref. [23] where it was used effectively for estimating γ_1 and γ_{11} using PERM simulations in the cubic half-lattice. See also Refs. [16–18].

Two dimensions: In the square half-lattice, the best estimate of μ_2 [see Eq. (2)] was used in Eq. (16). The top panel of Fig. 1 shows the data for self-avoiding walks grafted to the hard wall (these are 10-stars in our notation) with entropic exponent $\gamma_1\equiv\gamma_{10}$. The middle curve shows the confidence interval on the data as a shaded envelope. There are odd-even parity effects in these plots, but they were dealt with by only plotting data for even values of n.

The best estimate of γ_1 was obtained fixing its value to straighten the graph in Fig. 3. An error bar on the best estimate was determined by varying the value of γ_1 to produce the other curves in the figure. These curves are either convex or concave as the y axis is approached, and this curving becomes apparent when γ_1 is changed by $\epsilon=0.00020$ in either direction. Thus, we select as our error bar on γ_1 this value of ϵ, giving our best estimate

$$\gamma_1=0.95325\pm0.00020. \tag{17}$$

The estimate for γ_{11} was similarly obtained using the data of grafted self-avoiding walks with their endpoints in the hard wall forming a surface loop (these are 11-stars in our notation). The results of the analysis are shown in the bottom panel of Fig. 3. Our best estimate is

$$\gamma_{11}=-0.1875\pm0.0020. \tag{18}$$

With these results, one may test Barber's scaling relation. This gives

$$2\gamma_1-\gamma_{11}=2.094\pm0.003. \tag{19}$$

The exact value is $\gamma+\nu=43/32+3/4=67/32=2.09375$. The absolute difference from the estimate above is 0.00025, a factor of 10 smaller than the stated error bar of 0.003. This result is a strong numerical verification of Barber's scaling relation in two dimensions. The remaining data for 2-stars and 3-stars were similarly analyzed to obtain estimates of the exponents γ_{21^g} and γ_{31^g}. The results are shown in Table II. Observe that there are no numerical estimates

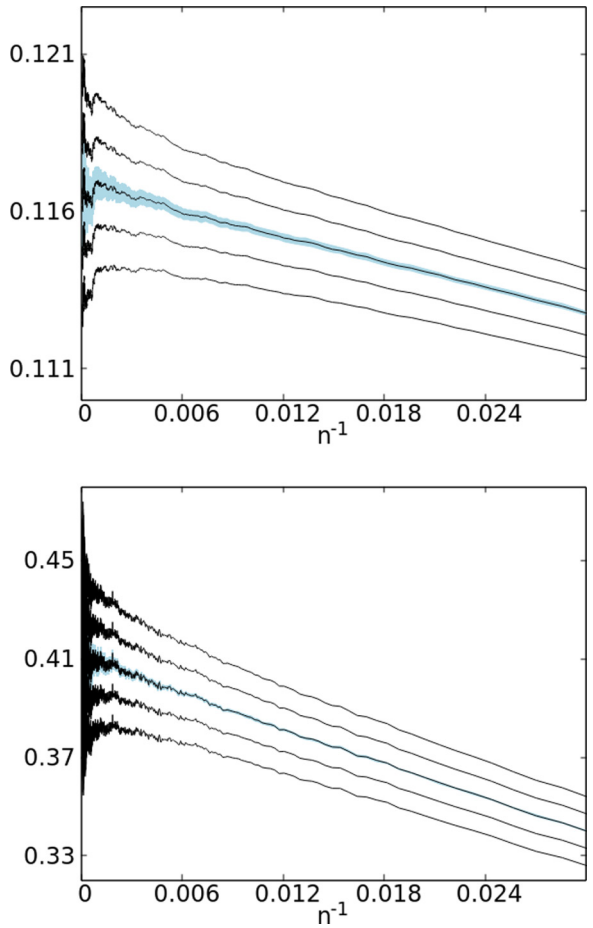

FIG. 3. Determining γ_1 and γ_{11} in the square lattice by plotting the left-hand side of Eq. (16) as a function of $1/n$. The middle curve is obtained by selecting that value of the exponent giving a straight line. In each panel a shaded envelope (more visible in the top panel) on the middle curve gives the confidence interval on the raw data. (Top panel) The middle curve is plotted with $\gamma_1 = 0.95325$ against $1/n$. A confidence interval $\sigma = 0.00020$ is obtained by adding and subtracting σ from γ_1. The top two curves have an increasing upwards tendency as the y axis is approached, and the bottom two curves similarly have a downwards tendency. This gives the best (rounded) estimate $\gamma_1 = 0.9533 \pm 0.0002$. (Bottom panel) A similar analysis to determine γ_{11}. This gives $\gamma_{11} = -0.188 \pm 0.002$.

in the literature for these exponents. These estimates are consistent, within error bars, with the (known) exact values in two dimensions. This both confirms, on the one hand, that the exact results are correct, and on the other hand, that the numerical methods in this paper produce high quality estimates of the entropic exponents. Testing Eq. (13) using our numerical values give

$$2\,\gamma_{21} - \gamma_{211} = 0.348 \pm 0.034, \tag{20}$$

and the exact value of $\gamma - 1 = 11/32 = 0.34375$ is well inside the stated error bar. The estimate for γ_{20} also verifies the identity in Eq. (12).

The exceptional case is for 3111-stars, namely 3-stars with their central node at the origin in the square half-lattice and with each arm from the central node having its endpoint in the hard wall (see Fig. 2). In this case, the data were too sparse to analyze. In general, very few 3111-star conformations were encountered in our simulation because one arm will have to be accommodated inside a surface loop formed by another and the hard wall (as illustrated schematically in Fig. 2). Plotting the few data points obtained for 3111-stars gave a graph which is not inconsistent with the exact value $\gamma_{3111} = -4.25$.

TABLE II. Half square lattice entropic exponents.

$\gamma_{\mathcal{G}}$	Exact	Literature	This work
γ_1	0.953125	0.945(5) [31] 0.9551(3) [33]	0.9533(2)
γ_{11}	−0.1875	−0.19(3) [31]	−0.188(2)
γ_{20}	0.34375		0.344(1)
γ_{21}	−0.796875		−0.796(2)
γ_{211}	−1.9375		−1.94(3)
γ_{211}	−1.9375		−1.94(5)[a]
γ_{211}	−1.9375		−1.93(4)[b]
γ_{30}	−0.828125		−0.827(2)
γ_{31}	−1.96875		−1.969(4)
γ_{311}	−3.109375		−3.11(1)
γ_{3111}	−4.25		−4.25(5)[a]

[a]Calculated by Eq. (11).
[b]Calculated by Eq. (13).

A numerical estimate of γ_{3111} can be obtained from the other three 3-star exponents using Eq. (11), namely

$$\gamma_{3111} = \gamma_{30} - 3\,\gamma_{31} + 3\,\gamma_{311} = -4.25 \pm 0.05, \tag{21}$$

where we used the results in Table II, and added the error bars to find a confidence interval.

Overall, one can conclude that Eq. (9), and the exact values of the entropic exponents in two dimensions, are supported by our numerical results.

Three dimensions: In the cubic lattice, corrections to scaling are dominated by the confluent correction term which is of the form C/n^{Δ} [see Eq. (15)]. There is a competing, faster decaying, analytic correction B/n, or even higher order confluent corrections, which may impact an analysis using Eq. (16), in particular at small values of n. Our approach here is based on the methods developed in Ref. [23], and we will be plotting the left hand of Eq. (16) against $n^{-\Delta}$ where Δ is fixed at its best estimate $\Delta = 0.528(8)$ [22]. Unlike in the square lattice, the confluent correction decays slowly, and competing higher order corrections may impact the analysis at small values of n. Therefore, the aim here is to find a linear plot at large values of n, discarding data at small n. In addition, there are, like in the square lattice, odd-even parity effects in the data, and we dealt with these by only plotting data for even values of n.

Plotting Eq. (16) to determine γ_1 gave graphs which were typically first concave (at small values of n) and then turning convex at large values of n. A linear graph can be obtained by making minor changes in the estimate of μ_3 and this gives the best estimate

$$\gamma_1 = 0.6745 \pm 0.0008. \tag{22}$$

This estimate was obtained by determining that value of γ_1 that straightens the graph when Eq. (16) was plotted using the data. In this case, its final value was insensitive to small changes in the value of μ_3 from its best estimate in Eq. (3), and

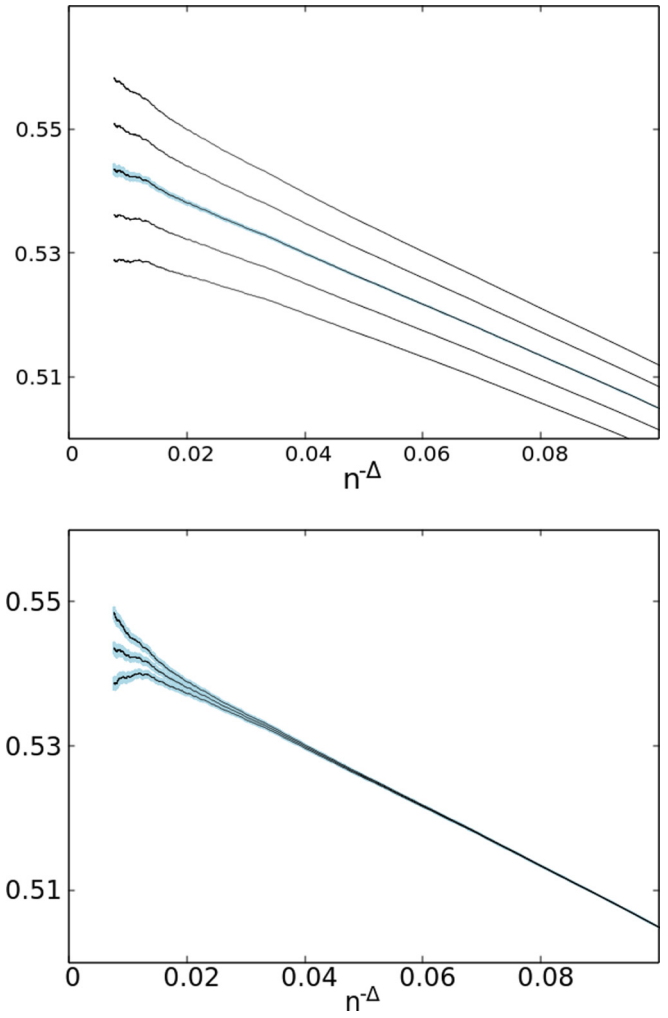

FIG. 4. Determining the best value of γ_1. In the top panel, Eq. (16) was plotted with $\Delta = 0.528$ and $\mu_3 = 4.684039931 - \delta$, where $\delta = 2.3 \times 10^{-6}$. The effect of minor changes in the plots due to changes in μ_3 are shown in the bottom panel. The top curve is for μ_3 equal to its best value in Eq. (3), the middle curve for $\mu_3 - \delta$, and the bottom curve for $\mu_3 - 2\delta$.

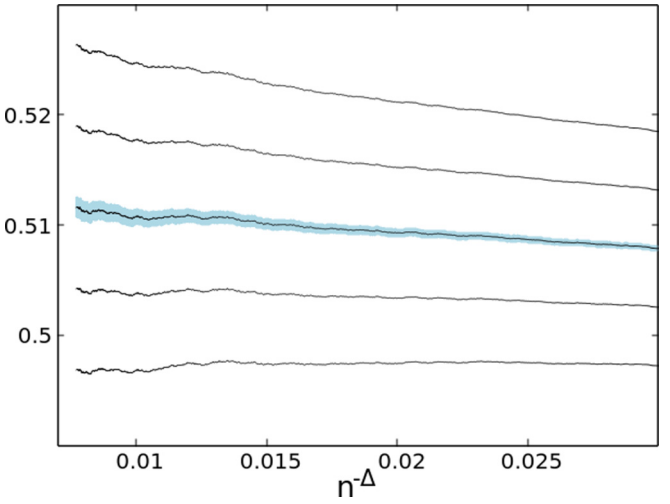

FIG. 5. Determining the best value of γ_1. The middle curve is a plot of Eq. (16) as a function of $1/n^{\Delta} \in [0.007, 0.03]$ with $\Delta = 0.528$ and $\mu_3 = 4.684039931$. This gives the estimate $\gamma_1 = 0.6785(8)$. The top two graphs are plotted using $\gamma_1 + k\epsilon$ with $k = 1, 2$ where $\epsilon = 0.0008$, while the bottom two are plots with $k = -1, -2$.

also with small changes in Δ within its error bars. However, it was not possible to find a straight graph of the data without changing the value of μ_3 in minor ways from that in Eq. (3). Following the approach in Ref. [23], the effects of these small changes in μ_3 are shown in the bottom panel of Fig. 4, where our data are plotted with γ_1 fixed at its best value in Eq. (22), but with the growth constant fixed at $\mu_3 - k\,\delta$ where $k = 0, 1, 2$ and $\delta = 2.3 \times 10^{-6}$. If $k = 0$, then the curvature is upwards as the y axis is approached. The bottom downwards curvature is seen for $k = 2$, while the best fit is for $k = 1$.

These results do *not* imply that the estimate in Eq. (3) is suspect, but instead expose limitations in the data in this paper—if the purpose was to estimate μ_3 from the data obtained here, then one would at best expect to do this to an accuracy of $O(2.3 \times 10^{-6})$. In addition, changing μ_3 from its best value introduces an extra degree of freedom in the analysis, and may give biased estimates of the exponents. In order to avoid this possibility, we fixed the value of μ_3 at its best known estimate, and then proceeded with curve fitting while discarding data at small values of n.

The analysis giving the estimate in Eq. (22) relies almost exclusively on data with $0.02 \leqslant n^{-\Delta} \leqslant 0.10$ (as seen in the bottom panel of Fig. 4). This corresponds to $78 \leqslant n \leqslant 1650$, while data with $n > 1650$ are compensated by the small change in the value of μ_3. This, however, cannot be the best way of extracting a good estimate of γ_1, and more care is needed. In particular, one should rely on large values of n in the analysis, since corrections to scaling are reduced with increasing n. In addition, changes in the value of μ_3 introduces an additional degree of freedom in the analysis, and it primarily affects data at large n. Thus, the analysis was repeated, but without changes in the value of μ_3, and discarding data with $n \leqslant 766$. This gives the results in Fig. 5. The middle curve corresponds to the best estimate of γ_1:

$$\gamma_1 = 0.6785 \pm 0.0008. \tag{23}$$

The two top curves are convex, while the two bottom curves are concave, and give the estimated error bar above. Since this estimate is based on data for larger values of n, it is taken as the best estimate of this exponent.

We have listed our best estimate for $\gamma_1 = 0.6785(8)$ in Table III, where we also compare it to earlier estimates in the literature. The best available estimate is in Ref. [37]. This estimate excludes our best estimate from its (very small) error bar. Conversely, that estimate is well within the error bar in Eq. (23). Sources of a systematic error in our estimate may be due to the choice of the random number generator (in this paper we used the mersenne twistor for 64 bit architecture [45]), or due to limitations in carrying significant digits along in the simulation [we used long double (80-bit) precision in the C programming language]. We also used gnuplot [49] to analyze the data, and it also has finite precision. We avoided large numbers in our simulation by only storing the ratio

TABLE III. Half cubic lattice entropic exponents.

$\gamma_{\mathcal{G}}$	ϵ^1-approx	Literature	This work
γ_1	0.625	0.679(2)[36]	0.6785(8)
		0.687(5)[34,35]	
		0.6786(12) [23]	0.6765(8)[c]
		0.677667(17) [37]	
γ_{11}	−0.463	−0.383(5) [36]	−0.389(3)
		−0.38(2) [34,35]	
		−0.390(2) [23]	−0.390(3)[c]
		−0.389245(28) [37]	
γ_{20}	0.125	0.15698(34)[d] [19,26]	0.154(3)
		0.15695300(95)[d] [27]	
γ_{21}	−0.963		−0.918(8)
γ_{211}	−2.050		−2.02(8)
γ_{211}	−2.050		−1.99(2)[a]
γ_{211}	−2.050		−1.99(2)[b]
γ_{30}	−0.500		−0.521(2)
γ_{31}	−1.588		−1.59(2)
γ_{311}	−2.675		−2.68(7)
γ_{3111}	−3.763		−3.9(6)
γ_{3111}	−3.763		−3.8(2)[a]
γ_{40}	−1.250		−1.325(4)
γ_{41}	−2.338		−2.406(8)
γ_{411}	−3.425		−3.48(4)
γ_{4111}	−4.513		−4.6(2)
γ_{41111}	−5.600		−5.8(1.1)[a]
γ_{50}	−2.125		−2.243(4)
γ_{51}	−3.213		−3.318(7)
γ_{511}	−4.300		−4.41(4)
γ_{5111}	−5.388		−5.5(2)

[a]Calculated by Eq. (11).
[b]Calculated by Eq. (13).
[c]Panneton random number generator [46].
[d]Estimations using Eq. (12).

$s_n^{(f)}(g)/\mu_3^n$ in our programs and data files. Repeated division by μ_3 during the simulation may also introduce rounding errors which accumulate during the simulation.

The value of the surface loop exponent γ_{11} was similarly estimated (Fig. 6). The best estimate consistent with our data is

$$\gamma_{11} = -0.389 \pm 0.003. \tag{24}$$

Barber's scaling relation can be tested in three dimensions by the results in Eqs. (22) and (24). The best available estimate of the numerical estimate of the metric exponent of self-avoiding walks is $\nu = 0.58759700(40)$ [22,38] and of the entropic exponent $\gamma = 1.15695300(95)$ [27]. Adding these gives $\gamma+\nu = 1.7445500(14)$. Our results give

$$2\,\gamma_1 - \gamma_{11} = 1.746(5). \tag{25}$$

This result includes the sum $\gamma + \nu$ inside its error bar, and so is consistent with the Barber scaling relation in three dimensions.

These results were retested by performing simulations using an alternative random number generator (the Panneton generator [46]). The results are shown in Table III where $\gamma_1 = 0.6765(8)$ and $\gamma_{11} = -0.390(3)$. This gives $2\gamma_1 - \gamma_{11} = 1.743(5)$, again consistent with the Barber scaling relation and with Eq. (25).

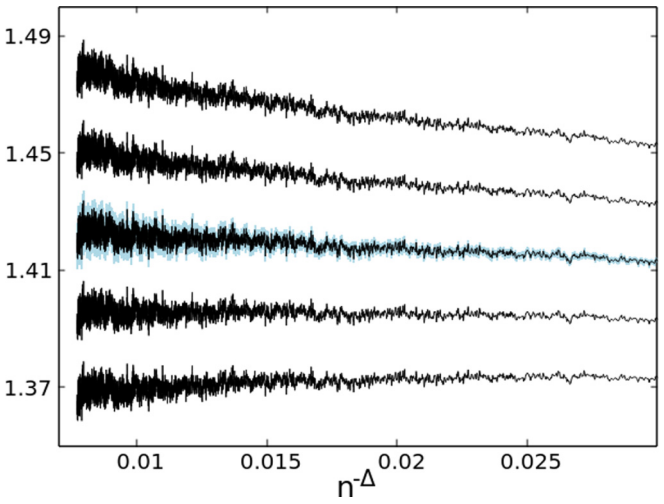

FIG. 6. Determining the best value of γ_{11}. The middle curve is a plot of Eq. (16) as a function of $1/n^{\Delta}$ with $\Delta = 0.528$ and $\mu_3 = 4.684039931$. This gives the estimate $\gamma_{11} = -0.3893$. The top two graphs are plotted using $\gamma_{11} + k\epsilon$ with $k = 1, 2$ where $\epsilon = 0.0030$, while the bottom two are plots with $k = -1, -2$.

Plotting our data for grafted f-stars with $2 \leqslant f \leqslant 5$ produced graphs which do not straighten at the best value of γ_{f1^g}. Instead, the locus of the data points were typically concave at small values of n, even as it straightens as n increases. This again suggests that higher order corrections to scaling are complicating the analysis. Since the slowest decaying correction is C/n^{Δ}, and it becomes dominant as n is increased, the exponents were estimated by focusing on the largest values of n as before. That is, by using Eq. (16), the exponent is estimated by setting it to straighten the curve at the largest values of n, even if there is a remaining curvature seen at the smallest values of n.

In Fig. 7, the result for γ_{20} is shown. These graphs were obtained by using the best estimate obtained from our data

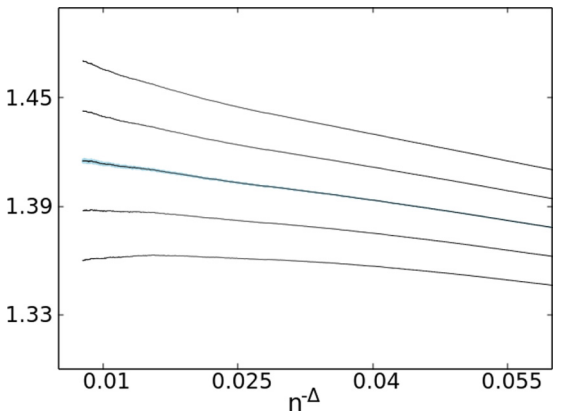

FIG. 7. Estimating γ_{20} by plotting the left hand side of Eq. (16) as a function of $n^{-\Delta}$ for $206 \leqslant n \leqslant 10000$. The middle graph corresponds to the best esimate $\gamma_{20} = 0.154 \pm 0.003$, while the top two curves and the bottom two curves, are used to determine the confidence interval.

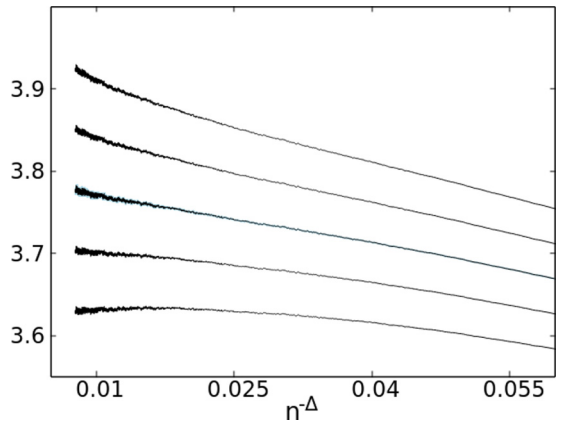

FIG. 8. Plotting Eq. (16) against $n^{-\Delta}$ for $573 \leqslant n \leqslant 10\,000$ to determine γ_{21}.

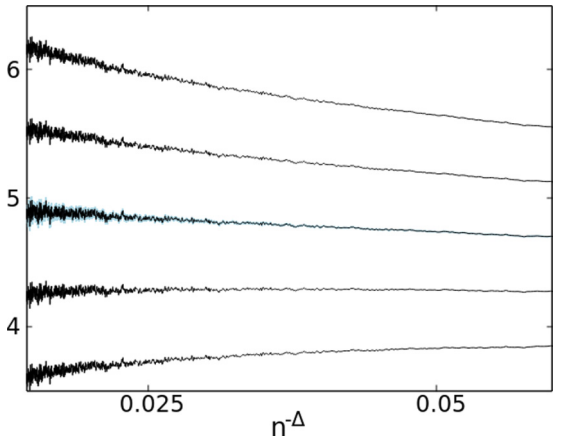

FIG. 9. Plotting Eq. (16) against $n^{-\Delta}$ for $37 \leqslant n \leqslant 2946$ to determine γ_{211}.

and give

$$\gamma_{20} = 0.154 \pm 0.003. \tag{26}$$

The best estimate of γ_{20} in the literature is obtained by noting from Eq. (12) that $\gamma_{20} = \gamma - 1$ and using the best estimate $\gamma = 1.15695300(95)$ [27]. This shows that $\gamma_{20} = 0.15695300(95)$, and this is well within the stated error bar of the estimate in Eq. (26). Conversely, these results also support the identity in Eq. (12) in three dimensions.

The analysis for γ_{21} is shown in Fig. 8. These graphs are for $573 \leqslant n \leqslant 10000$. Observe that there remains a minor concavity in the middle curve at the largest values of $n^{-\Delta}$ but that the curves straigthen as $n^{-\Delta}$ decreases when n approaches $n = 10,000$. The top two curves are convex, and the bottom two curves are concave. This gives the best value of γ_{21}:

$$\gamma_{21} = -0.918 \pm 0.008. \tag{27}$$

The estimates of γ_{20} and γ_{21} in Eqs. (25) and (27) can be used to predict γ_{211} using Eq. (11). This gives

$$\gamma_{211} = 2\,\gamma_{21} - \gamma_{20} = -1.99 \pm 0.02. \tag{28}$$

Determining γ_{211} directly from the data is complicated by poor sampling at large n. Examination of the data shows reasonable sampling for $n \leqslant 2500$, and poor sampling for $n \geqslant 3000$. Plotting Eq. (16) for $37 \leqslant n \leqslant 2846$ gives Fig. 9, which unambiguously gives the estimate

$$\gamma_{211} = -2.02 \pm 0.08 \tag{29}$$

with a conservatively determined error bar (there is significant curvature present in the second and fourth curves in Fig. 9). This result is consistent with the estimated value in Eq. (28). Using this result with the estimate of γ_{21} gives $2\gamma_{21} - \gamma_{211} = 0.18(10)$. Within its large error bar, this result is consistent with $\gamma = 1.15695300(95)$ [27] as shown by Eq. (13).

The estimates for grafted 2-star exponents are listed in Table III.

Data for grafted 3-, 4-, and 5-stars were similarly analyzed and the results appear in Table III. In the case of grafted 3-stars, the estimates are

$$\begin{aligned} \gamma_{30} &= -0.521 \pm 0.002, \\ \gamma_{31} &= -1.59 \pm 0.02, \\ \gamma_{311} &= -2.68 \pm 0.07, \\ \gamma_{3111} &= -3.9 \pm 0.6. \end{aligned} \tag{30}$$

The estimate for γ_{3111} is based on data for $206 \leqslant n \leqslant 1080$. These results are consistent with Eq. (11). Using Eq. (11) and the estimates for γ_{30}, $\gamma_{31,}$ and γ_{311} gives a better estimate of γ_{3111} instead:

$$\gamma_{3111} = \gamma_{30} - 3\,\gamma_{31} + 3\,\gamma_{311} = -3.8 \pm 0.3, \tag{31}$$

and this result is still consistent with the estimate of γ_{3111} in Eq. (30).

The data for grafted 4-stars give

$$\begin{aligned} \gamma_{40} &= -1.325 \pm 0.004, \\ \gamma_{41} &= -2.406 \pm 0.008, \\ \gamma_{411} &= -3.48 \pm 0.04, \\ \gamma_{4111} &= -4.6 \pm 0.2. \end{aligned} \tag{32}$$

The estimate for γ_{4111} is based on $206 \leqslant n \leqslant 1650$. By Eq. (11),

$$\gamma_{41111} = -\gamma_{40} + 4\,\gamma_{41} - 6\,\gamma_{411} + 4\,\gamma_{4111} = -5.8 \pm 1.1. \tag{33}$$

Finally, for grafted 5-stars

$$\begin{aligned} \gamma_{50} &= -2.251 \pm 0.003, \\ \gamma_{51} &= -3.333 \pm 0.007, \\ \gamma_{511} &= -4.41 \pm 0.04, \\ \gamma_{5111} &= -5.5 \pm 0.2. \end{aligned} \tag{34}$$

Our sampling of 51111- and 511111-stars were too poor to allow estimates of the entropic exponents.

III. CONCLUSIONS

The purpose of this paper was to estimate the entropic exponents of half-space grafted f-stars, and to numerically

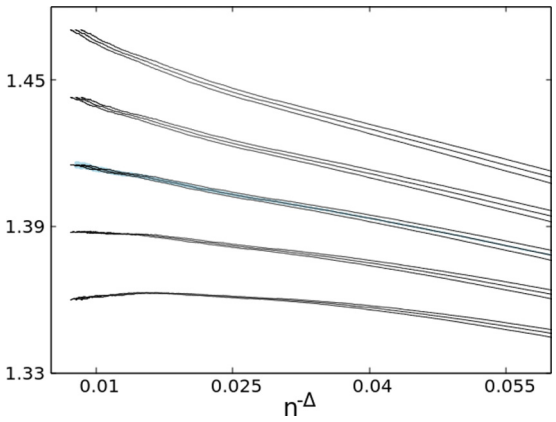

FIG. 10. Estimating the effect of the uncertainty in Δ. The data in Fig. 7 is replotted here, but now with $\Delta \in \{0.520, 0.528, 0.536\}$. In each case, the shift in the curves are very small compared to changes when the data are plotted using $\gamma_{20} = 0.254 \pm \epsilon$ for $\epsilon \in \{0.003, 0.006\}$. This shows that any change in the estimate of γ_{20} due to the uncertainty in Δ is small compared to the stated error bar in Table III.

verify some relations involving these exponents. Our results are shown in Tables II and III, Barber's scaling relation is tested in Eqs. (19) and (25), and Eqs. (12) and (13) were tested in Eqs. (20) and (26). The relation in Eq. (13) was similarly tested for grafted 2-stars and 3-stars in the half cubic lattice [Eqs. (28), (29), (30), and (31)]. In all respects, the general framework using vertex exponents σ_f and surface vertex exponents σ'_f in Eq. (5) is strongly supported by the numerical results here.

The estimates of exponents in three dimensions listed in Table III were obtained by assuming that the confluent exponent has value $\Delta = 0.528$, giving the curves shown in Figs. 4–9. The best numerical estimate of the confluent exponent is $\Delta = 0.528(8)$ [22], and the uncertainty in this estimate may have an impact on the estimated exponents in Table III. This was investigated by replotting those graphs for values of Δ at the boundaries of its confidence interval. For example, in Fig. 10, the data in Fig. 7 are replotted but using three values for the confluent exponent, namely $\Delta \in \{0.520, 0.528, 0.536\}$. The graph shows that the resulting curves corresponding to $\Delta = 0.520$ and $\Delta = 0.536$ are displaced in minor ways from the curve corresponding to the central value $\Delta = 0.528$. The displacements of the curves are small when compared to the distance separating the five curves in Fig. 7 corresponding to $\gamma_{20} = 0.154 \pm \epsilon$, where $\epsilon \in \{0, \pm 0.003, \pm 0.006\}$. This shows that the size of the effect due to the uncertainty in Δ is small when compared to the size of the uncertainty in our estimate of γ_{20} in Table III. Similar results were obtained for the other exponents in Table III.

The results in two dimensions are consistent to good accuracy with the exact (conformal invariance) values of the exponents. This not only provides strong evidence supporting the theoretical analysis of the surface entropic exponents for uniform branched networks in two dimensions in Refs. [19–21,32], but also shows that the numerical methods used in this paper (and in Refs. [14,16,23,36]) are sound. This enhances confidence in the cubic lattice results shown here, which cannot be verified against a list of exact values. On the contrary, few of the surface exponents of grafted lattice stars in three dimensions have been calculated before (as can be seen in Table III), apart from the $O(\epsilon)$-expansion estimates which give good, but not excellent, agreement with the numerical estimates obtained in this paper.

ACKNOWLEDGMENTS

E.J.J.vR. acknowledges financial support from NSERC (Canada) in the form of Discovery Grant No. RGPIN-2019-06303 and is in debt to N. Clisby for useful feedback on an earlier version of the manuscript.

[1] J. M. Hammersley and K. W. Morton, Poor man's Monte Carlo, J. Roy. Stat. Soc. Ser. B (Meth) **16**, 23 (1954).
[2] S. R. Broadbent and J. M. Hammersley, Percolation processes I. crystals and mazes, Math. Proc. Camb. Phil. Soc. **53**, 629 (1957).
[3] C. E. Soteros, Lattice models of branched polymers with specified topologies, J. Math. Chem. **14**, 91 (1993).
[4] S. G. Whittington and C. E. Soteros, Uniform branched polymers in confined geometries, Macromol. Rep. **29**, 195 (1992).
[5] M.-N. Chee and S. G. Whittington, The growth constant of uniform star polymers in a slab geometry, J. Phys. A: Math. Gen. **20**, 4915 (1987).
[6] N. Clisby and I. Jensen, A new transfer-matrix algorithm for exact enumerations: Self-avoiding polygons on the square lattice, J. Phys. A: Math. Theor. **45**, 115202 (2012).
[7] J. L. Jacobsen, C. R. Scullard, and A. J. Guttmann, On the growth constant for square-lattice self-avoiding walks, J. Phys. A: Math. Theor. **49**, 494004 (2016).
[8] N. Clisby, Calculation of the connective constant for self-avoiding walks via the pivot algorithm, J. Phys. A: Math. Theor. **46**, 245001 (2013).
[9] A. Miyake and K. F. Freed, Internal chain conformations of star polymers, Macromolecules **17**, 678 (1984).
[10] J. E. G. Lipson, S. G. Whittington, M. K. Wilkinson, J. L. Martin, and D. S. Gaunt, A lattice model of uniform star polymers, J. Phys. A: Math. Gen. **18**, L469 (1985).
[11] J. Batoulis and K. Kremer, Thermodynamic properties of star polymers: Good solvents, Macromolecules **22**, 4277 (1989).
[12] B. Duplantier and A. J. Guttmann, Statistical mechanics of confined polymer networks, J. Stat. Phys. **180**, 1061 (2020).
[13] K. Ohno and K. Binder, Monte Carlo simulation of many-arm star polymers in two-dimensional good solvents in the bulk and at a surface, J. Stat. Phys. **64**, 781 (1991).
[14] P. Grassberger, Nonuniform star polymers in two dimensions, J. Phys. A: Math. Gen. **27**, L721 (1994).

[15] K. Ohno, Scaling theory and computer simulation of star polymers in good solvents, Cond. Mat. Phys. **5**, 15 (2002).
[16] H.-P. Hsu, W. Nadler, and P. Grassberger, Scaling of star polymers with 1-80 arms, Macromolecules **37**, 4658 (2004).
[17] S. Campbell and E. J. Janse van Rensburg, Numerical estimates of square lattice star vertex exponents, Phys. Rev. E **103**, 052137 (2021).
[18] S. Campbell and E. J. Janse van Rensburg, Lattice star and acyclic branched polymer vertex exponents in 3d, J. Phys. A: Math. Theor. **55**, 015002 (2022).
[19] B. Duplantier, Polymer Network of Fixed Topology: Renormalization, Exact Critical Exponent γ in Two Dimensions, and $d = 4-\epsilon$, Phys. Rev. Lett. **57**, 941 (1986).
[20] B. Duplantier, Statistical mechanics of polymer networks of any topology, J. Stat. Phys. **54**, 581 (1989).
[21] B. Nienhuis, Coulomb gas description of 2-D critical behaviour, J. Stat. Phys. **34**, 731 (1984).
[22] N. Clisby and B. Dünweg, High-precision estimate of the hydrodynamic radius for self-avoiding walks, Phys. Rev. E **94**, 052102 (2016).
[23] P. Grassberger, Simulations of grafted polymers in a good solvent, J. Phys. A: Math. Gen. **38**, 323 (2005).
[24] B. Duplantier and H. Saleur, Exact Surface and Wedge Exponents for Polymers in Two Dimensions, Phys. Rev. Lett. **57**, 3179 (1986).
[25] R. Guida and J. Zinn-Justin, Critical exponents of the n-vector model, J. Phys. A: Math. Gen. **31**, 8103 (1998).
[26] R. D. Schramm, G. T. Barkema, and R. H. Bisseling, Exact enumeration of self-avoiding walks, J. Stat. Mech: Theo. Expr. (2011) P06019.
[27] N. Clisby, Scale-free Monte Carlo method for calculating the critical exponent γ of self-avoiding walks, J. Phys. A: Math. Theor. **50**, 264003 (2017).
[28] L. Schäfer, C. von Ferber, U. Lehr, and B. Duplantier, Renormalization of polymer networks and stars, Nucl. Phys. B **374**, 473 (1992).
[29] V. Schulte-Frohlinde, Y. Holovatch, C. von Feber, and A. Blumen, Interactions between star polymers: Higher-order calculations of the scaling exponents, Cond. Mat. Phys. **6**, 703 (2003).
[30] M. N. Barber, Scaling relations for critical exponents of surface properties of magnets, Phys. Rev. B **8**, 407 (1973).
[31] M. N. Barber, A. J. Guttmann, K. M. Middlemiss, G. M. Torrie, and S. G. Whittington, Some tests of scaling theory for a self-avoiding walk attached to a surface, J. Phys. A: Math. Gen. **11**, 1833 (1978).
[32] J. L. Cardy, Conformal invariance, in *Phase Transitions and Critical Phenomena*, edited by C. Domb and J. L. Lebowitz (Academic Press, London, 1987), Vol. 11, pp. 55–126.
[33] H. Meirovitch and I. Chang, Surface critical exponents of self-avoiding walks on a square lattice with an adsorbing linear boundary: A computer simulation study, Phys. Rev. E **48**, 1960 (1993).
[34] S. Livne and H. Meirovitch, Computer simulation of long polymers adsorbed on a surface I. Corrections to scaling in an ideal chain, J. Chem. Phys. **88**, 4498 (1988).
[35] H. Meirovitch and S. Livne, Computer simulation of long polymers adsorbed on a surface II. Critical behavior of a single self-avoiding walk, J. Chem. Phys. **88**, 4507 (1988).
[36] R. Hegger and P. Grassberger, Chain polymers near an adsorbing surface, J. Phys. A: Math. Gen. **27**, 4069 (1994).
[37] N. Clisby, A. R. Conwar, and A. J. Guttmann, Three-dimensional terminally attached self-avoiding walks and bridges, J. Phys. A: Math. Theor. **49**, 015004 (2016).
[38] N. Clisby, Accurate Estimate of the Critical Exponent ν for Self-Avoiding Walks Via a Fast Implementation of the Pivot Algorithm, Phys. Rev. Lett. **104**, 055702 (2010).
[39] K. Binder, C. Domb, and M. S. Green, Critical behaviour at surfaces, in *Phase Transitions and Critical Phenomena*, edited by C. Domb and J. L. Lebowitz (Academic Press, London, 1983), Vol. 8, pp. 1–144.
[40] K. Binder and D. P. Landau, Critical phenomena at surfaces, Physica A **163**, 17 (1990).
[41] P. Grassberger, Pruned-enriched Rosenbluth method: Simulations of θ polymers of chain length up to 1,000,000, Phys. Rev. E **56**, 3682 (1997).
[42] H.-P. Hsu and P. Grassberger, A review of Monte Carlo simulations of polymers with perm, J. Stat. Phys. **144**, 597 (2011).
[43] T. Prellberg and J. Krawczyk, Flat Histogram Version of the Pruned and Enriched Rosenbluth Method, Phys. Rev. Lett. **92**, 120602 (2004).
[44] S. Campbell and E. J. Janse van Rensburg, Parallel PERM, J. Phys. A: Math. Theor. **53**, 265005 (2020).
[45] M. Matsumoto and T. Nishimura, Mersenne twister: A 623-dimensionally equidistributed uniform pseudo-random number generator, ACM Trans. Model. Comput. Simul. **8**, 3 (1998).
[46] F. Panneton, P. L'Ecuyer, and M. Matsumoto, Improved long-period generators based on linear recurrences modulo 2, ACM Trans. Math. Softw. **32**, 1 (2006).
[47] B. Nienhuis, Exact Critical Point and Critical Exponents of O(n) Models in Two Dimensions, Phys. Rev. Lett. **49**, 1062 (1982).
[48] S. Caracciolo, A. J. Guttmann, I. Jensen, A. Pelissetto, A. N. Rogers, and A. D. Sokal, Correction-to-scaling exponents for two-dimensional self-avoiding walks, J. Stat. Phys. **120**, 1037 (2005).
[49] T. Williams, C. Kelley *et al.*, Gnuplot 4.6: An interactive plotting program, http://gnuplot.sourceforge.net/ (2013).